

A TOOL ORIENTATION SMOOTHING METHOD FOR FIVE-AXIS MACHINING TO AVOID SINGULARITY PROBLEMS

CHUANHUI CUI

*School of Mechanical Engineering and Automation, Beihang University, Beijing, China, and
Collaborative Innovation Center for Advanced Aero-Engine, Beihang University, Beijing, China, and
Dongchang College of Liaocheng University, Liaocheng, China*

ZHENGQING ZHU

*School of Mechanical Engineering and Automation, Beihang University, Beijing, China, and
Collaborative Innovation Center for Advanced Aero-Engine, Beihang University, Beijing, China
e-mail: by18071104@buaa.edu.cn*

SHUAI CHEN

School of Mechanical Engineering and Automation, Beihang University, Beijing, China

QIANG ZHENG, JINFENG CHAI, XIANCAI LI

AECC South Industry Company Limited, ZhuZhou, China

In numerically controlled grinding of aeroengine blades, a sharp change in a rotating shaft caused by a singular zone greatly reduces grinding precision and quality. This paper proposes an algorithm to optimize the tool-path that combines optimization of the C -axis rotation angle, a modification to the tool orientation and adjustments to the tool position by taking a four-array machine tool with two rotational axes (B -axis and C -axis) as an example. The algorithm was verified using VERICUT software, furthermore, in machining experiments, the rotation amplitudes of the rotary axis in singular areas was effectively reduced, which ensured grinding quality of blades.

Keywords: aeroengine blade, smoothness of tool orientation, five-axis machine tool, singular area

1. Introduction

As blades play an important role in aeroengines, their surface accuracy and integrity greatly influence their fatigue life and aerodynamic performance under service environments. Therefore, blades are generally ground and polished to ensure surface integrity and accuracy in their final shape (Huang *et al.*, 2016; Chen and Zhao, 2015). The fixed-track grinding of blades with a super-abrasive elastic grinding wheel can solve grinding problems for hard-to-manufacture features, such as the leading edge, exhaust edge and the filet to realize complete blade grinding. However, it is important to avoid the interference between the tool axis and edge plates and to realize blade-body grinding without tool markings while machining blades with upper- and lower-edge plates. Therefore, tool orientation without the interference is generally specified at the upper- and lower-edge plates of blades based on shape parameters of the tool, whereas the planning of tool orientation is performed by the computer-aided machining (CAM) system through an interpolation vector (Ma *et al.*, 2015). As shown in Fig. 1a, due to the upper-edge plate, the tool orientation v_u is inclined to the right relative to the blade axis when the grinding tool is near the upper-edge plate of the blade in the blade grinding process. As shown in Fig. 1d, due to the lower-edge plate, the tool orientation v_l is inclined to the left relative to the blade axis when the grinding tool is near the lower-edge plate of the blade. As shown in Figs. 1b and 1c, due to

the opposite inclination direction of the tool position at the upper- and lower-edge plates, the tool orientation will be approximately parallel to the axis of the blade when the grinding tool is machining the middle part of the blade. If the blade axis is parallel to the axis of the machine tool turntable during the five-axis grinding process, singular areas from the five-axis computerized numerical control (CNC) machine tool inevitably occur during processing (Pal, 2005). In singular areas, the tool orientation is approximately parallel to the axis of the machine tool turntable for the five-axis tool, which causes small fluctuations in the tool orientation leading to large variations in the rotation shaft of the machine tool. This significantly increases the non-linear errors of the machine tools, worsens the processing state in these areas, and can even cause machining scrap (Chen *et al.*, 2020). Therefore, optimizing the five-axis tool-path in singular areas is essential to improve the machining precision and surface quality.

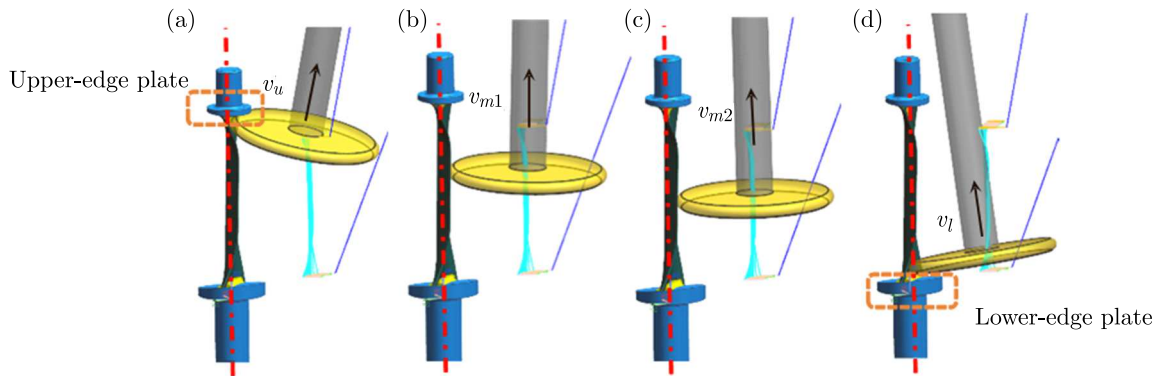


Fig. 1. The grinding process of the blade with the upper- and lower-edge plates: (a) attitude of tool orientation relative to the blade when machining the upper-edge plate, (b) attitude of the tool relative to the blade when machining the middle of the blade, (c) attitude of the tool relative to the blade when machining the middle of the blade, (d) attitude of tool orientation relative to the blade when machining the lower-edge plate

The existing five-axis machining singularity-avoidance method can be performed in two stages tool-path planning and post-processing without changing the workpiece clamping form (Cripps *et al.*, 2017; Wang, 2007) or rotating shaft configuration (Anotaipaboon *et al.*, 2006). In the tool-path planning stage, singular regions can be avoided by optimizing the tool orientation. Affouard *et al.* (2004), Yang and Altintas (2013) and Wan *et al.* (2018) fitted the tool orientation for each tool position into spline curves and fine-tuned the control points to ensure that the tool orientation avoided the singular region of the five-axis machine tool, which improved the smoothness of the tool orientation. Castagnetti *et al.* (2008) and Lin *et al.* (2014, 2016) defined the feasible region of the tool orientation and optimized it within the feasible region to avoid singular regions and obtain better machining quality. Wang (2012) optimized the tool position in the singular region by monitoring the angle between the tool orientation and the rotation axis. Tajima and Sencer (2020) avoided singular regions through real-time path planning. Lartigue *et al.* (2004) and Lu *et al.* (2016) modified the tool-path by adjusting the control points for side milling, which improved the smoothness of the rotating shaft near the singular points and ensured machining accuracy. In the post-processing stage, Sørby (2007) modeled kinematics of a non-orthogonal machine tool and fine-tuned motion of the rotating axis near the singular point in post-processing to improve the robustness of the tool-path in the singular regions. It is noted that such a method inevitably introduces machining errors when adjusting motion of the rotating shaft. Munlin *et al.* (2004) reduced motion errors near singular points through the shortest-path planning during post-processing. Wang *et al.* (2008) and Chen *et al.* (2020) improved the machining accuracy of singular regions through linear interpolation.

In the planning stage of tool-path, the singular problem of tool-path can be realized by combining the structure of the machine tool. However, at present, the universal CAM system does not have this function, so it needs to carry on a secondary development based on the development interface provided by CAM, which is difficult to realize and is characterized by poor versatility. In the post-processing stage, the smoothness of the tool-path in singular regions is improved, and the non-linear errors in these areas are reduced by fine-tuning of motion of the rotating shaft, shortest-path planning and interpolation. However, the problem of an excessive rotation amplitude for the rotating shaft in singular regions is not fundamentally solved, and fine-tuning of motion introduces new machining errors. Interpolation causes machine-tool feed fluctuations due to tool points that are too dense, and this affects the machining efficiency and quality.

In this study, an algorithm to optimize the tool-path that combines optimization of the C -axis rotation angle, a modification of the tool orientation and adjustment to the points is proposed by taking a four-array machine tool with two rotational axes (B and C) as an example based on the previous research. This method improves the smoothness of the tool-path in the singular region, and the effectiveness of this method is proved by experiments.

2. Algorithm research

2.1. Overall algorithm flow

A flow chart of the overall algorithm is shown in Fig. 2, and it shows the following steps. Step 1: post-process the original tool-path data. Step 2: obtain tool-path segments located in the singular region based on the normal Z component of the tool position and fluctuations of the C -axis. Step 3: adjust the swing angles of the B -axis and C -axis corresponding to the tool position in the singular area based on the angular travel of the C -axis at the beginning and end of the tool rail section in the singular area so that these axes rotate uniformly. Step 4: smooth the B -axis and C -axis swing angles of the tool positions before and after the beginning and end points of the singular tool rail section to ensure connection between the singular section and the front and rear sections. Step 5: adjust tool orientation corresponding to the tool position according to the adjusted B -axis and C -axis swing angles. Step 6: calculate the tool position based on the adjusted tool orientation combined with the contact position, normal vector of the contact and cutter parameters. Step 7: reprocess the adjusted tool-path data after processing its position data in all singular areas to complete the tool-axis smoothing.

2.2. Kinematic analysis of the machine tool

The machine tool used in this study is a four-spindle rectangular array five-axis machine tool to achieve blade grinding and grinding, whose one rotary axis (C -axis) is on the table and the other one (B -axis) on the spindle, as shown in Fig. 3a. The tool is a drum-shaped tool, as shown in Fig. 3b. The coordinate system of the five-axis machine tool with a swing head and turntable is shown in Fig. 3c. The $O_W X_W Y_W Z_W$, $O_M X_M Y_M Z_M$, and $O_T X_T Y_T Z_T$ sets of axes are the coordinate systems of the workpiece, machine, and tool, respectively, and point B is the rotation center of the B -axis. The rotation center of the C -axis coincides with the origin of the workpiece coordinate system. The vector B is the tool coordinate origin O_T in the machine coordinate system relative to the coordinates of point B . The initial coordinates of the tool in the coordinate system are $P_t^T(0, 0, 0, 0, 0, 1)$. The coordinate of point P_t^T in the workpiece coordinate system should be consistent with the corresponding tool position $P_n^W(x_n, y_n, z_n, i_n, j_n, k_n)$ after coordinated movements for each machine tool axis (Geng *et al.*, 2018). If $(mx_n, my_n, mz_n, mb_n, mc_n)$

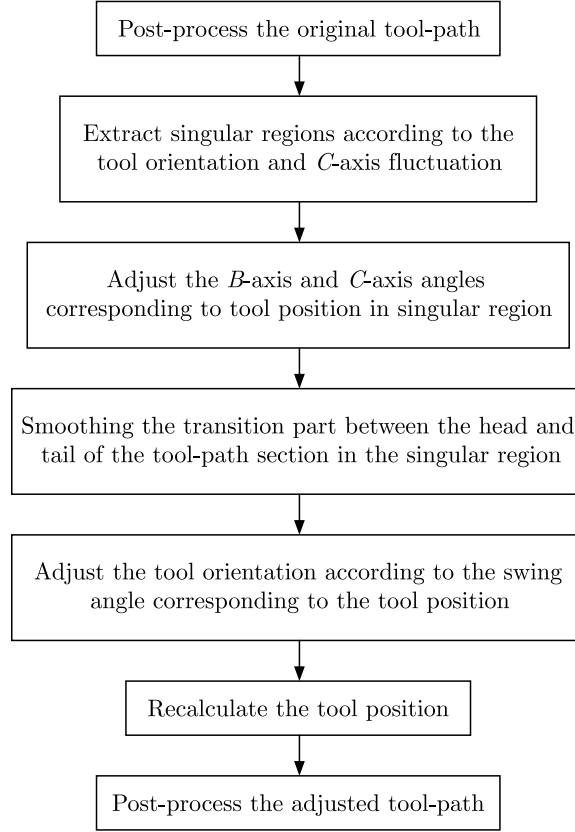


Fig. 2. Overall flow of the proposed algorithm

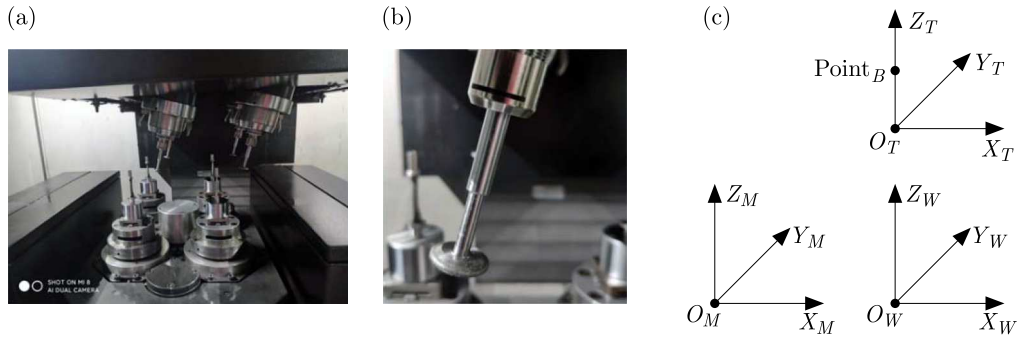


Fig. 3. (a) Four-spindle rectangular array five-axis machine tool, (b) drum-shaped tool, (c) coordinate system of the five-axis machine tool with a swing head and turntable: $O_W X_W Y_W Z_W$, $O_M X_M Y_M Z_M$, and $O_T X_T Y_T Z_T$ sets of axes are the coordinate systems of the workpiece, machine and tool, respectively, and point_B is the rotation center of the *B*-axis

are the coordinates of the corresponding axes of the machine tool in the component coordinate system, there is a transformation relation as shown as

$$P_n^W = P_t^T \text{Trans}(\text{vector}_B) \text{Rot}(B, mb_n) \text{Trans}(m_x, m_y, m_z) \text{Rot}(C, mc_n) \quad (2.1)$$

When solving motion for each axis of the machine tool in reverse, the expansion of Eq. (2.1) gives two cases for motion of the *B*-axis and *C*-axis of the machine tool as

$$mb_{n1} = \arccos(k_n)$$

$$mc_{n2} = \begin{cases} \arctan(j_n/i_n) & i_n \geq 0 \\ 90^\circ \text{sgn}(j_n) - \arctan(j_n/i_n) & i_n < 0 \end{cases} \quad (2.2)$$

or

$$mb_{n2} = -\arccos(k_n)$$

$$mc_{n2} = \begin{cases} \arctan(j_n/i_n) & i_n \leq 0 \\ \arctan(j_n/i_n) - 90^\circ \operatorname{sgn}(j_n) & i_n > 0 \end{cases} \quad (2.3)$$

Equation (2.4) is used to calculate the total rotations Δ_1 and Δ_2 of the B and C axes corresponding to the two solutions, and the smaller value is selected as the current solution

$$\Delta_1 = |mb_{n1} - mb_{n-1}| + |mc_{n1} - mc_{n-1}|$$

$$\Delta_2 = |mb_{n2} - mb_{n-1}| + |mc_{n2} - mc_{n-1}| \quad (2.4)$$

2.3. Determination of the singular area

Because the singularity problem is only related to the direction of the tool axis and not to the position of the tool, only the relationship between the rotation axis and the direction of the tool axis needs to be solved. The tool orientation $v_n(i_n, j_n, k_n)$ is a unit vector which satisfies $i_n^2 + j_n^2 + k_n^2 = 1$, therefore, a unit sphere (radius of the sphere has unit length, and it is commonly referred to as a Gaussian sphere in which each point corresponds to a blade-axis direction) is taken as an example. As shown in Fig. 4a, the tool orientation is expressed by v , the center point of the axis is located at the center of the sphere, and the end points are distributed on the sphere. Figure 4b shows a top-down view, which indicates that the initial position of v is parallel to the Z -axis, i.e., $v = (0, 0, 1)$, based on the analysis in Section 2.2. The included angle between any two tool orientations v_1 and v_2 on the unit circle is set as φv_1 and can reach v_2 in two simultaneous steps: firstly, rotation by α degrees around the Y -axis to v_m , and then rotation by β degrees around the Z -axis to v_2 .

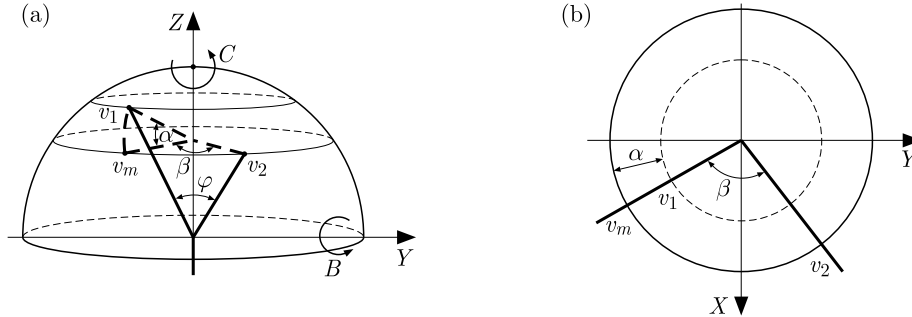


Fig. 4. (a) Gaussian sphere, (b) its top view

According to Eqs. (2.2) and (2.3), when k_n is equal to 1, b_n is 0 and c_n can be any value; this is called a singular point of the tool-path. At this time, the C -axis rotation angle corresponding to the previous tool position is taken as c_n to avoid the singular-point problem. When k_n approaches but is not equal to 1, small changes of i_n and j_n result in large changes in the C -axis rotation angle. Therefore, the singular area discrimination threshold is set as ε , while the corresponding $k_n, k_{n+1}, \dots, k_{n+m}$ for each tool position and the size of ε are determined successively. The track segment of the tool that is continuously less than ε is the track segment in the singular area. Through a large number of experiments and analysis, ε is set from 0.9848 to 0.9962 (3° - 5° corresponding to the swing angle of the B -axis).

To explain the machine-tool singularity phenomenon more intuitively, Fig. 5a shows the tool pose at two adjacent positions of the tool in the grinding process of the middle part of the blade body of the example blade. The tool orientations at the two adjacent tool positions are v_1 and v_2 , respectively. As shown in Fig. 4b, the tool orientations are represented on the Gaussian

sphere O (O is the center of the Gaussian sphere), the circle O_s is a small-diameter circle with the Z -axis near the north pole on the surface of the Gaussian sphere O , which corresponds to a smaller conical angle φ ($\leq 10^\circ$). The tool orientations v_1 and v_2 are on the circle O_s , and the angle φ between v_1 and v_2 is less than φ , which meets the maximum in the five-axis machining path-planning stage. However, as shown in Fig. 5c, in the top view of the Gaussian sphere O , \dot{v}_1 is the projection of v_1 onto the XOY plane, \dot{v}_2 is the projection of v_2 onto the XOY plane, $\angle \dot{v}_1 O \dot{v}_2$ is the projection of $\angle v_1 O v_2$ onto the XOY plane, the $\angle \dot{v}_1 O \dot{v}_2$ is obviously larger than the $\angle v_1 O v_2$, which produces a singularity phenomenon when the tool-path is from v_1 to v_2 . The maximum angle of the C -axis can reach 90° in one cycle, which is much larger than the maximum allowable angle in a single cycle. For a five-axis machine tool with two rotational axes (B and C), singularity problems may occur only when the tool orientation appears in a circle with a smaller radius at the north pole for the Gaussian sphere, which is usually called a singular area.

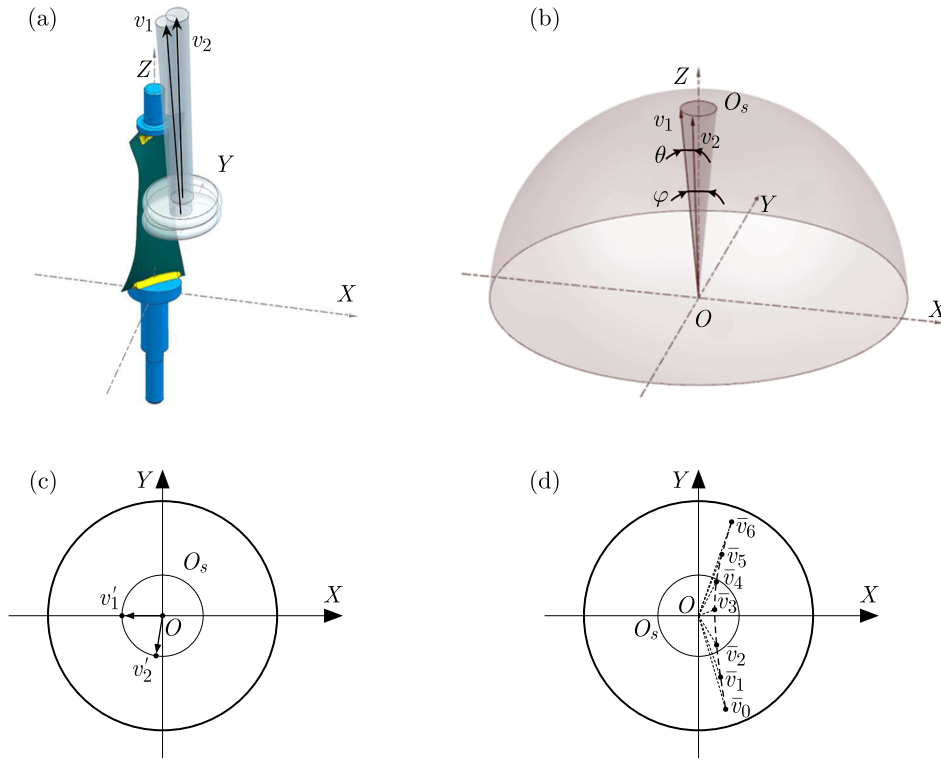


Fig. 5. Generation mechanism of a singular cone: (a) relationship between the tool and workpiece pose, (b) singular cone and tool orientations in the singular cone, (c) top view of the Gaussian sphere and C -axis rotation angle corresponding to the tool orientation in the singular area, (d) singularity of the machine tool in the C -axis

To further illustrate the singularity of the machine tool, the top view of the Gaussian sphere O (O is the center of the Gaussian sphere) is shown in Fig. 5d, where the circle O_s is the singular cone, and $\bar{v}_0, \bar{v}_1, \dots, \bar{v}_6$ are continuous tool orientations, connecting the lines between O and each of the tool orientations. The angle between two adjacent lines is the angle of C -axis of the machine tool between two adjacent tool points when the machine tool is running. It can be seen from the figure that during transformation of the tool orientation from \bar{v}_1 to \bar{v}_5 , the C -axis changes greatly. In this case, the tool-path segment from \bar{v}_1 to \bar{v}_5 is a singular tool-path segment. Here \bar{v}_1 is the first tool point corresponding to the tool orientation before the tool-path enters the singular region, \bar{v}_5 is the first tool point corresponding to the tool orientation after the tool-path leaves the singular region. In order to better describe the algorithm in this paper,

\bar{v}_1 is defined as the tool head orientation of the singular tool-path segment, and \bar{v}_5 is the tail of the tool orientation of the singular tool-path segment.

2.4. Normal vector adjustment principle of tool position

According to distribution of the head and tail of the singular tool-path segment, the tool orientations in the singular region are adjusted in two cases. In the first case, the projection angle of the tool orientation corresponding to the head and tail points in the singular area is less than 90° in the top view of the Gaussian sphere. As shown in Fig. 6a, v_1^1, v_2^1, v_3^1 and v_4^1 are tool orientations corresponding to the tool position points in the singular area, v_0^1 is the tool orientation corresponding to the tool position before the tool-path enters the singular area, and v_5^1 is the tool orientation corresponding to the first tool position after the tool-path leaves the singular area, with $\angle v_0^1 O v_5^1$ being less than 90° . During the movement of the cutter shaft from v_0^1 to v_5^1 , the C -axis of the machine tool rotates significantly, which causes a singularity problem. The shortest line connection is between points v_0^1 and v_5^1 on the Gaussian sphere surface. From $v_0^1, v_1^1, v_2^1, v_3^1, v_4^1$ and v_5^1 the distance relationship between the corresponding tool positions of v_1^1, v_2^1, v_3^1 and v_4^1 will correspond to the adjustments in the connection of v_0^1 and v_5^1 on the connecting line. As shown in Fig. 6b, the amplitudes of motion for the B -axis and C -axis of the machine tool are remarkably small and uniform as the tool position is changed from v_0^1 to v_5^1 , which avoids singular problems in the machining process.

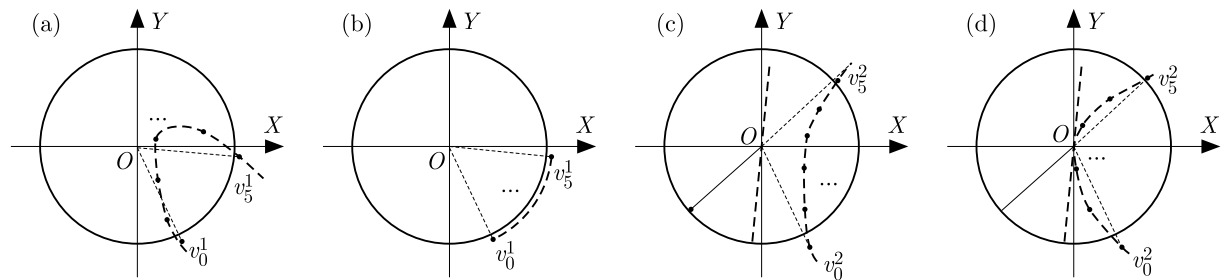


Fig. 6. According to the projection angle, different strategies are adopted to adjust tool orientation in the singular region: (a) projection angle less than 90° of tool orientation before the adjustment, (b) projection angle less than 90° of tool orientation after the adjustment, (c) projection angle greater than 90° of tool orientation before the adjustment, (d) projection angle greater than 90° of tool orientation after the adjustment

In the second case, the projection angle of the tool orientation corresponding to the head and tail points in the singular area is more than 90° based on the Gaussian sphere. As shown in Fig. 6c, the circle O_s is a top view of the singular cone, and v_1^2, v_2^2, v_3^2 and v_4^2 are the tool orientations corresponding to the tool positions in the singular area. v_0^2 is the tool orientation corresponding to the tool position before the tool-path enters the singular area, and v_5^2 is the tool orientation corresponding to the first tool position after the tool-path leaves the singular area. The graph shows that the C -axis of the machine tool rotates significantly as the tool position changes from v_0^2 to v_5^2 , which causes singularity problems. The shortest line connection is made between point v_0^2 , the north pole of the Gaussian sphere, and point v_5^2 on the surface of the Gaussian sphere. From $v_0^2, v_1^2, v_2^2, v_3^2, v_4^2$ and v_5^2 , the distance relationships between the corresponding tool positions are v_1^2, v_2^2, v_3^2 and v_4^2 , which corresponds to the adjustments in the connecting line from v_0^2 to v_5^2 . As shown in Fig. 5d, the amplitudes of motion for the B -axis and C -axis are remarkably small and uniform as the tool position is changed from v_0^2 to v_5^2 , which avoids singularity problems in the machining process.

2.5. Adjustment algorithm of swing angle corresponding to tool position in a singular region

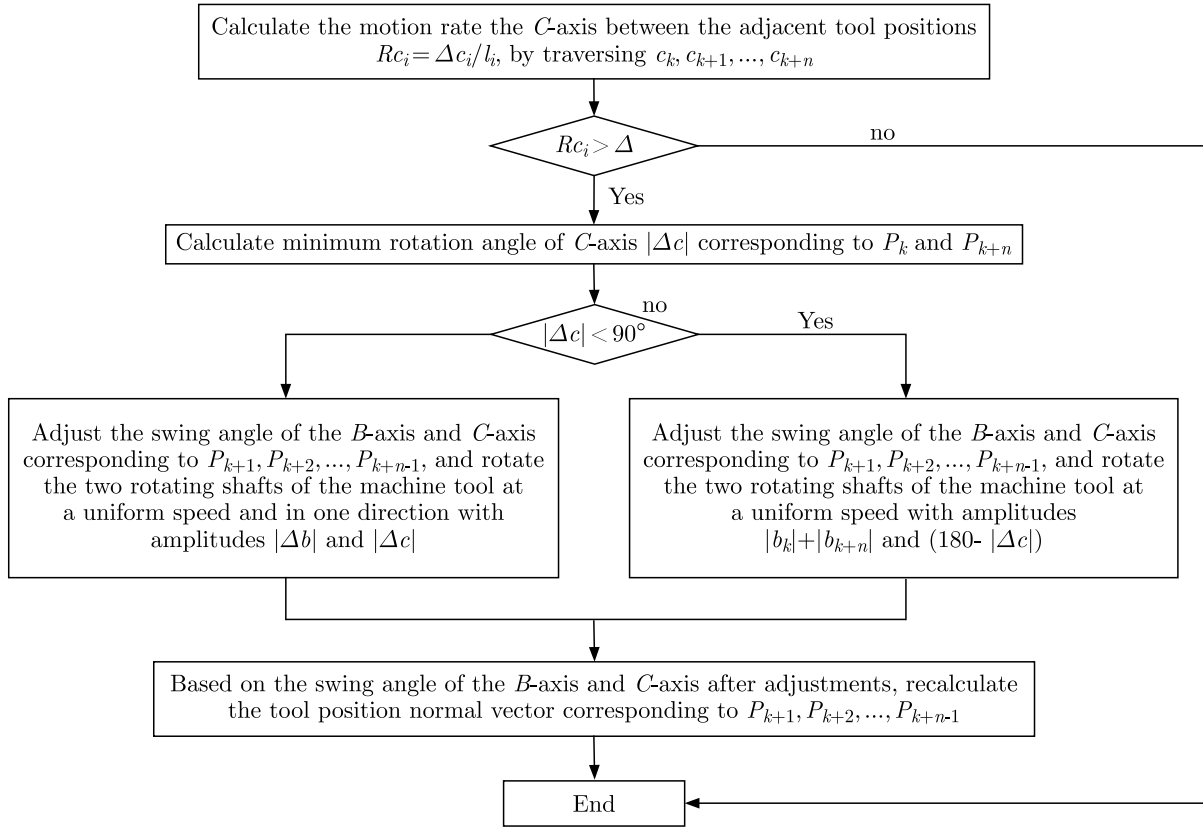


Fig. 7. Adjustment process of the tool orientation in a singular region

Figure 7 shows a flow chart of the tool-position normal-vector adjustment algorithm in a singular region. P_k is the starting point of the tool-path segment in the singular region, P_{k+n} is the end point, and the rotation angles of the axis are $b_k, b_{k+1}, \dots, b_{k+n}$ and $c_k, c_{k+1}, \dots, c_{k+n}$. The tool-path length l_i corresponding to each tool point is calculated in turn with P_k as the starting point. Then, P_{k+i} is calculated for each tool position corresponding to $t_i = l_i / \sum l_i$. Therefore, the procedure to adjust the tool orientation is as follows.

1. Calculate the rotation angle of the C -axis between the adjacent tool positions $\Delta c_i = c_{k+i} - c_{k+i-1}$, and then calculate the motion rate of the C -axis between the adjacent tool positions $Rc_i = \Delta c_i / l_i$ by traversing $c_k, c_{k+1}, \dots, c_{k+n}$, where $i = 1, 2, \dots, n$. If the value of Rc_i ($i = 1, 2, \dots, n$) is too large to indicate that there is a large fluctuation in the C -axis in this singular region, the threshold value θ of the C -axis is preset when the program is executed, θ is set to 1-3 in a lot of experimental analysis, judge whether $Rc_i > \theta$ ($i = 1, 2, \dots, n$) is established. If yes, perform Step 2; otherwise, the singular region is not necessary for optimization, and the program is stopped.
2. Set $i = 1$; calculate the effective motion stroke of the C -axis and B -axis during the machining stage from P_k to P_{k+n} . The effective travel of the C -axis is then $\Delta c = c_{k+n} - c_k$, and that of the B -axis is $\Delta b = b_{k+n} - b_k$ when $|\Delta c| > 180^\circ$. Step 3 is performed by adding or subtracting $m \times 360$ so that Δc is in the range -180° to 180° .
3. Judge whether $|\Delta c| \leq 90^\circ$ is valid. If $|\Delta c|$ remains unchanged, carry out Step 4; otherwise, implement Step 5.
4. If $\Delta b_{k+i} = \Delta b \times t_i$, $\Delta c_{k+i} = \Delta c \times t_i$; perform Step 11.
5. If $\Delta c > 90^\circ$, $\Delta c = -(180 - \Delta c)$, e.g., $\Delta c < -90^\circ$, $\Delta c = 180 + \Delta c$; perform Step 6.

6. If $\Delta c_h = |\Delta c|/2$, $\Delta c_{k+i} = \Delta c \times t_i$; perform Step 7.
7. Judge whether $|\Delta c_{k+i}| \leq \Delta c_h$ is true. If true, execute Step 8; otherwise, skip to Step 9.
8. $\Delta b_{k+i} = 2 \times b_k \times t_i$; perform Step 11.
9. $\Delta b_{k+i} = b_k + 2 \times b_{k+n} \times (t_i - 0.5)$; perform Step 10.
10. If $\Delta c_{k+i} \geq 0$ is true, then $\Delta c_{k+i} = \Delta c_{k+i} + 180^\circ$; otherwise $\Delta c_{k+i} = \Delta c_{k+i} - 180^\circ$, perform Step 11.
11. Determine whether $i = n$ is true. If true, the adjustment process is over; otherwise, $i = i + 1$ and move to Step 3.

2.6. The change of head and tail normal vectors for the tool-path in singular regions by smoothing

After adjusting the tool orientation in a singular region, the relationship that describes the original normal vector variations for the tool position is changed so that the swing angles of the B -axis and C -axis mutations occur at the boundary transition of the singular region. Figures 8a and 8b, respectively, show changes in the tool orientation corresponding to the tool position before and after tool-orientation adjustments along the cutter track section in the singular region. There is a sudden change in the normal vector of the tool axis at tool positions v_2 and v_7 , which correspond to the head and tail of the tool-path section in the adjusted singular region. If this is left untreated, speed fluctuations will appear when the machine tool operates here, which will affect the machining quality.

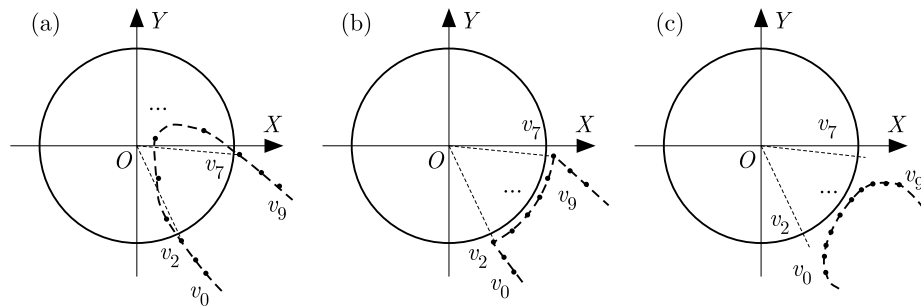


Fig. 8. Smoothing of the head and tail normal vectors for the tool-path in singular regions: (a) normal projection of tool orientation before the adjustment, (b) normal projection of tool orientation after the adjustment, (c) normal vector projection of tool orientation after the smoothing

As shown in Fig. 8b, there are two front tool positions P_0 and P_1 , and two rear tool positions P_3 and P_4 corresponding to the tool position P_2 , which takes the length of the tool-path section as a parameter. Then, the swing angles of the B -axis and C -axis corresponding to the five tool sites are fitted to quadratic Bezier curves using the least-squares method, which is then inversely calculated based on the corresponding parameters of each tool site for P_1 , P_2 and P_3 . The tool-axis smoothing at the head of the tool-path section in the singular region is then completed based on the corresponding swing angle of the B -axis and C -axis.

Taking the swing angle of the B -axis as an example, the specific processing approach is explained starting from P_0 . The corner of b_i ($i = 0, 1, \dots, 4$), which corresponds to the normal vector of each tool-position contact is calculated, and the tool-path length l_i corresponding to each tool position is calculated with P_0 as the starting point

$$l_i = \begin{cases} 0 & i = 0 \\ l_{i-1} + \text{dis}(P_i - P_{i-1}) & i = 1, 2, \dots, 4 \end{cases} \quad (2.5)$$

where $\text{dis}(P_i - P_{i-1})$ is the distance between P_{i-1} and P_i .

The value $t_i = l_i/l_4$ ($i = 0, 1, \dots, 4$) is taken as the corresponding b_i parameters. Refer to the description of quadratic B -spline in reference (Riesenfeld, 1975), the planning node vector $\mathbf{U}(0, 0, 0.5, 1, 1)$ is combined with t_i ($i = 0, \dots, 4$) to calculate the basis function corresponding to $N_{j,i}$ ($i = 0, \dots, 4$), where $j = 0, 1, 2, 3$ as

$$N_{j,0} = \begin{cases} 1 & u_j \leq t_i < u_{j+1} \\ 0 & \text{otherwise} \end{cases}$$

$$N_{j,p}(t_i) = \frac{t_i - u_i}{u_{i+p} - u_i} N_{j,p-1}(t_i) + \frac{u_{i+p+1} - t_i}{u_{i+p+1} - u_{i+1}} N_{j+1,p-1}(t_i) \quad (2.6)$$

$$\mathbf{E} = \begin{bmatrix} N_{0,2}(t_0) & \cdots & N_{2,2}(t_0) \\ \vdots & \ddots & \vdots \\ N_{0,2}(t_4) & \cdots & N_{2,2}(t_4) \end{bmatrix}$$

where b_i ($i = 0, \dots, 4$) is written in the form of the column vector $\mathbf{B} = [b_0, \dots, b_4]^T$. Equation (2.7) is used to solve each control point of the fitted B -spline, where $\mathbf{X} = [x_0, x_1, x_2]^T$, \mathbf{X} is a 3×1 matrix, x_0 , x_1 and x_2 are the values of B -spline control points

$$\mathbf{X} = (\mathbf{E}^T \mathbf{E})^{-1} \mathbf{E}^T \mathbf{B} \quad (2.7)$$

Finally, b_i ($i = 0, \dots, 4$) is fitted to a B -spline curve, which can be inversely calculated through the fitted spline curve of b_i ($i = 1, 2, 3$) to obtain smooth B -axis motion data.

2.7. Recalculation of tool position

The tool and workpiece surfaces have common normal vectors at the cutter contact point during machining. Therefore, the coordinates of the tool position (Xu and Chen, 2014) can be solved by combining the tool orientation and parameter information of the cutter when the normal vectors of the contact point are known. Commonly used tools for blade grinding and grinding are drum-shaped, as shown in Fig. 9. Given the tool diameter D , fillet radius R , contact point P_c , contact normal vector v_c , and normal vector of tool orientation v_0 , the tool position P_0 can be obtained from

$$P_1 = P_c + Rv_c \quad v_1 = v_0 \times (v_c \times v_0) \quad (2.8)$$

$$P_2 = P_1 + \left(\frac{D}{2} - R\right)v_1 \quad P_0 = P_2 - Rv_0$$

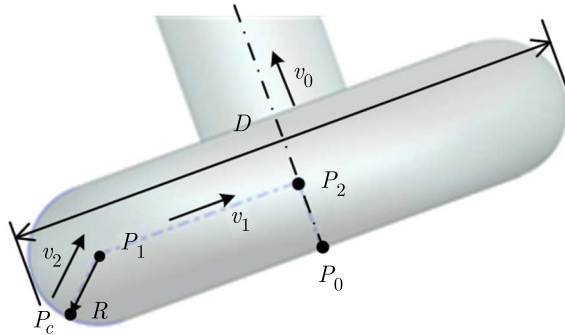


Fig. 9. Calculation of the normal vector for contact in a drum cutter

Similarly, for the commonly used ball cutters in milling, the radius R of the cutter, contact point P_c , contact normal vector v_c and tool orientation v_0 can be used to obtain the tool position P_0 from Eq. (2.8). The round-corner cutters commonly used in milling are similar

to drum cutters in that given the tool diameter D , radius R , contact point P_c , contact normal vector v_c and tool orientation v_0 , the tool position P_0 can be obtained from

$$P_0 = P_c + Rv_c - Rv_0 \quad (2.9)$$

Other commonly used tools can be derived in turn.

3. Verification example

As shown in Fig. 1, to realize full profile grinding of concave or convex surfaces with upper- and lower-edge plates in a certain model, the cutter shaft of the upper- (lower-) edge plate needs to tilt to the right (left) to avoid interfering with the cutter shaft. The cutter shaft in the middle is determined from the CAM system based on the interpolation of the built-in rules. Therefore, the blade-axis normal is nearly parallel to the blade axis when machining the middle part of the blade body. The blade axes are installed parallel to the C -axis of the rotating axes when a four-array machine tool has two rotational axes (B and C). Figure 10 shows the swing values

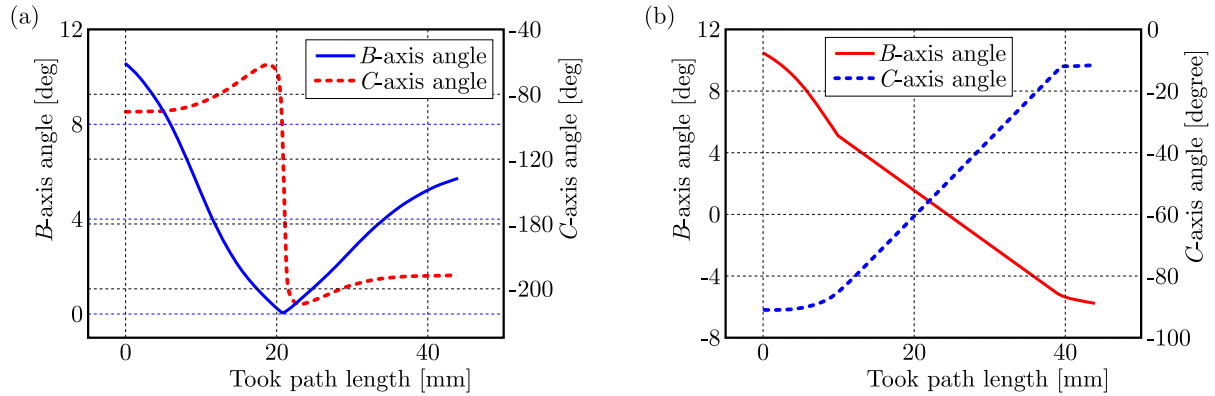


Fig. 10. Comparison of the B -axis and C -axis rotation angles (a) before and (b) after optimization

of the B -axis and C -axis corresponding to the fifth row of the tool-path in the program before and after optimization. Figure 10a indicates that the entire swing amplitude of the C -axis in the original tool-path is large with a sharp change. Meanwhile, there is a sudden change in the B -axis direction, which causes sharp acceleration and deceleration of the machine tool to produce large non-linear errors. Figure 10b shows the corresponding swings in the B -axis and C -axis after tool-path optimization. The total rotation angle of the C -axis is reduced significantly and the overall operation is smooth, while there is no sudden change in the direction of the B -axis. This can ensure smooth operation of the machine tool and plays a positive role in improving the processing quality.

It should be emphasized that because of the particularity of the structure of the array machine tool, the 840D numerical control system can not realize the RTCP function, so the machine tool is sensitive to the nonlinear error caused by the singular problem, and so the cutting simulation of the tool path before formal machining is particularly important. Cutting simulations were performed using the VERICUT software package, as illustrated in Fig. 11. In the simulation results, the light-yellow part of the blade is the surface of the workpiece, and the purple part is the surface of the workpiece after processing. From the simulation results shown in Fig. 11b, it can be clearly seen that when the tool-path is not optimized, large nonlinear errors are generated due to the singular region of the tool-path, which leads to a serious over-cutting problem, leading to the scrap of the processed workpiece. The simulation results in Fig. 11c show that there is no obvious over-cutting after optimization.

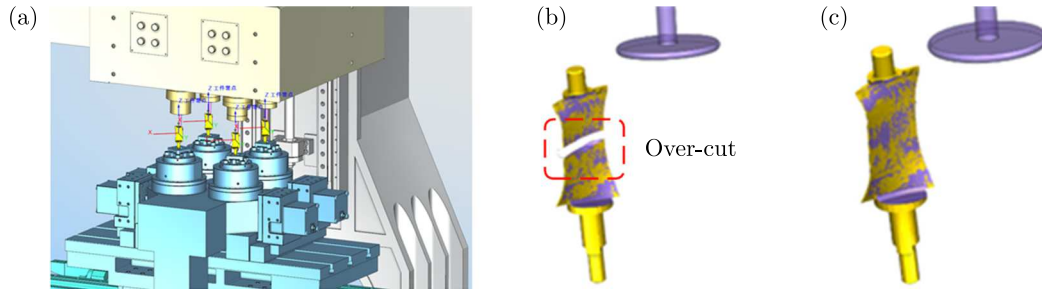


Fig. 11. VERICUT simulation model and its results, showing: (a) simulation model, (b) tool-path cutting simulation before optimization, (c) tool-path cutting simulation after optimization

In the grinding process, grinding process parameters directly affect quality of the surface processing of blades. Considering the surface profile and roughness requirements of titanium alloy fan blades, and combined with the experimental experience of grinding process parameter optimization in the early stage of our research group, the grinding processing parameters are shown in Table 1. A blade is machined using the optimized tool-path, as illustrated in Figs. 12a and 12b, and there is no undercut on the surface of the blade after machining. In the vertical section curve shown in Figs. 12a and 12b, 40 equidistant points are accurately detected with a coordinate-measuring machine which is equipped with a Renishaw SP25M contact scanning probe (Beijing, Hangruiwei PONY866, Metrolog XG13 contact measuring system, $MPE=(2.5+4L/1000)\mu m$ and the diameter of the probe is 1.5 mm). The results are shown in Fig. 12c, where the maximum surface error is less than 0.02 mm, which meets the design requirements (profile tolerance $-0.03\text{ mm}-+0.05\text{ mm}$). Therefore, it can be said that the proposed optimization method can meet the actual processing requirements.

Table 1. Grinding process parameters

	Convex	Concave	Leading-edge and trail-edge
Tool	D38r1.5 (Drum wheel)	D38r1.5 (Drum wheel)	D26r1.5 (Drum wheel)
Parameters	Speed 5000 r/min Feed 1200 mm/min Preloading 0.2 mm Single tool-path	Speed 5000 r/min Feed 1200 mm/min Preloading 0.2 mm Single tool-path	Speed 7000 r/min Feed 1000 mm/min Preloading 0.2 mm Single tool-path

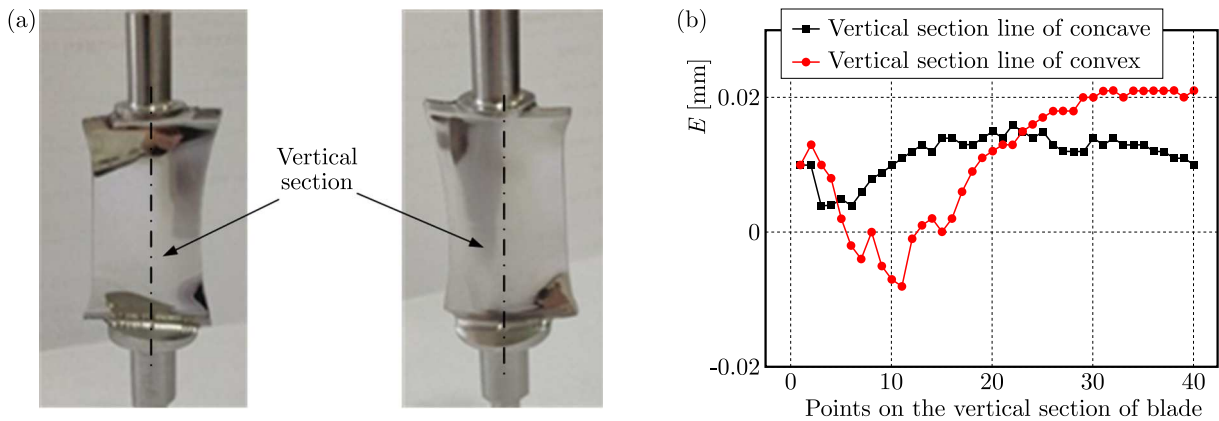


Fig. 12. Grinding effect on the back/basin surface of a double-ended blade model: (a) concave, (b) convex, (c) data for accuracy detection

4. Summary

To solve the problem of singular regions in the tool-path for five-axis grinding and grinding of full-profile aircraft-engine blades, a tool-path optimization algorithm that combines optimization of the B -axis and C -axis rotation angles, modifications of the tool-axis vectors and adjustments to the tool position is proposed in the post-processing stage of the tool-path. This method is easier to implement the tool orientation smoothing than the secondary development of CAM software.

The smoothness of the tool-path in singular regions is improved without interpolating or encrypting the original path. Problems such as rapid rotations of the rotating shaft in the singular regions and excessive non-linear errors are avoided. VERICUT simulation and actual processing verification can meet the actual machining requirements.

Funding

This work was supported by the National Science and Technology Major Project of the Ministry of Science and Technology of China (grant No. 2018ZX04004001).

References

1. AFFOUARD A., DUC E., LARTIGUE C., LANGERON J.M., BOURDET P., 2004, Avoiding 5-axis singularities using tool-path deformation, *International Journal of Machine Tools and Manufacture*, **44**, 4, 415-425
2. ANOTAIPAIBOON W., MAKHANOV S.S., BOHEZ E.L.J., 2006, Optimal setup for five-axis machining, *International Journal of Machine Tools and Manufacture*, **46**, 9, 964-977
3. CASTAGNETTI C., DUC E., RAY P., 2008, The domain of admissible orientation concept: A new method for five-axis tool-path optimization, *Computer-Aided Design*, **40**, 9, 938-950
4. CHEN G.L., ZHAO C.R., 2015, Digital production line of precision forging aeroengine blade (in Chinese), *Aeronautical Manufacturing Technology*, **22**, 78-83
5. CHEN L.J., WEI G.X., SUI Y.Z., WANG Z.Z., 2020, Non-linear error control method for five-axis machining singular zone, *Modular Machine Tool and Automatic Manufacturing Technique*, **3**, 111-113, 118
6. CRIPPS R.J., CROSS B., HUNT M., MULLINEUX G., 2017, Singularities in five-axis machining: Cause, effect and avoidance, *International Journal of Machine Tools and Manufacture*, **116**, 40-51
7. GENG C., WU Y., QIU J., 2018, Analysis of nonlinear error caused by motions of rotation axes for five-axis machine tools with orthogonal configuration, *Mathematical Problems in Engineering*, **2018**, 8, 1-16
8. HUANG Y., XIAO G.J., ZOU L., 2016, Current situation and development trend of grinding technology for blisk (in Chinese), *Acta Aeronautica et Astronautica Sinica*, **37**, 2045-2064
9. LARTIGUE C., TOURNIER C., RITOU M., DUMUR D., 2004, High-performance NC for HSM by means of polynomial trajectories, *CIRP Annals*, **53**, 1, 317-320
10. LIN Z.W., FU J.Z., SHEN H.Y., GAN W.F., 2014, Non-singular tool-path planning by translating tool orientations in C-space, *International Journal of Advanced Manufacturing Technology*, **71**, 9-12, 1835-1848
11. LIN Z.W., FU J.Z., SHEN H.Y., XU G.H., SUN Y.F., 2016, Improving machined surface texture in avoiding five-axis singularity with the acceptable-texture orientation region concept, *International Journal of Machine Tools and Manufacture*, **108**, 1-12
12. LU Y.A., BI Q.Z., ZHU L.M., 2016, Five-axis flank milling tool-path generation with smooth rotary motions, *Procedia CIRP*, **56**, 161-166

13. MA L., WANG H.X., ZHANG Y., 2015, Grinding parameters optimization for leading and trailing edge of aero-engine blade (in Chinese), *Modular Machine Tool and Automatic Manufacturing Technique*, **22**, 78-83
14. MUNLIN M., MAKHANOV S.S., BOHEZ E.L.J., 2004, Optimization of rotations of a five-axis milling machine near stationary points, *Computer-Aided Design*, **36**, 12, 1117-1128
15. PAL M., 2005, Random forest classifier for remote sensing classification, *International Journal of Remote Sensing*, **26**, 1, 217-222
16. RIESENFELD R.F., 1975, *Nonuniform B-Spline Curves*, 2nd ed. USA-JAPAN Conference Proceedings, 551-555
17. SØRBY K., 2007, Inverse kinematics of five-axis machines near singular configurations, *International Journal of Machine Tools and Manufacture*, **47**, 2, 299-306
18. TAJIMA S., SENCER B., 2020, Real-time trajectory generation for 5-axis machine tools with singularity avoidance, *CIRP Annals*, **69**, 1, 349-352
19. WAN M., LIU Y., XING W.J., ZHANG W.H., 2018, Singularity avoidance for five-axis machine tools through introducing geometrical constraints, *International Journal of Machine Tools and Manufacture*, **127**, 1-13
20. WANG D., CHEN Z.T., CHEN W.Y., 2008, Detection and control of non-linear errors in 5-axis machining (in Chinese), *J. Beijing Univ. Aeronaut. Astronaut.*, **34**, 9, 1003-1006, 1091
21. WANG L.N., 2012, Study on singular point problem in 5-axis NC machining (in Chinese), *Journal of Mechanical Engineering and Automation*, **5**, 122-124, 129
22. WANG R.Q., 2007, *Theoretical Research on Wide-Stripe NC Machining and its Application in Blade Machining* (in Chinese), Beijing: Beihang University, 156-189
23. XU R., CHEN Z., 2014, Method of five-axis tool radius compensation based on post-processor, *Journal of Mechanical Engineering*, **50**, 13, 157-164
24. YANG J.X., ALTINTAS Y., 2013, Generalized kinematics of five-axis serial machines with non-singular tool path generation, *International Journal of Machine Tools and Manufacture*, **75**, 119-132

Manuscript received May 29, 2022; accepted for print October 17, 2022